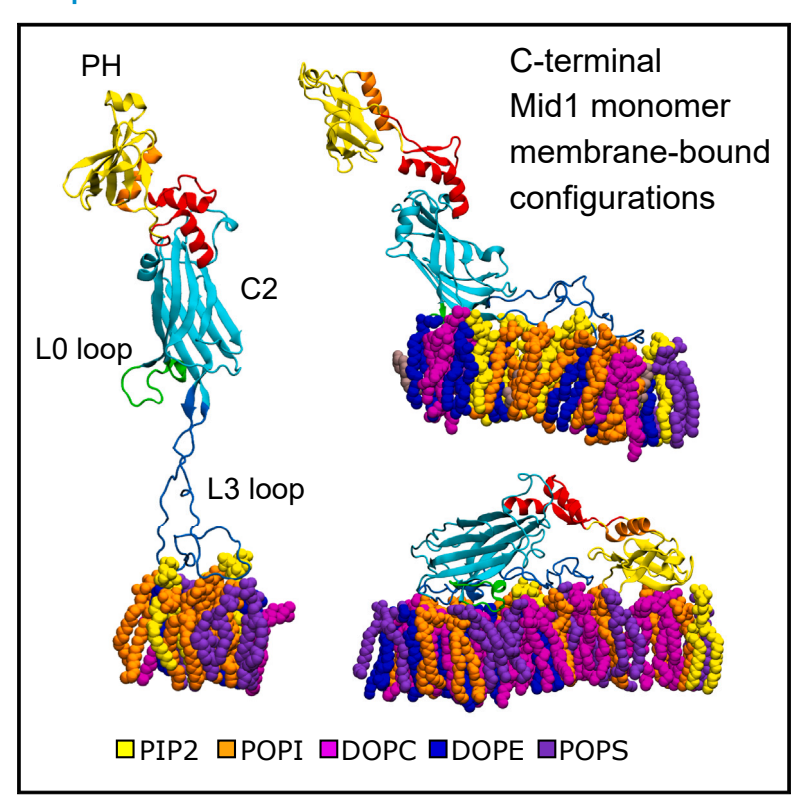
Structure

Anillin-related Mid1 as an adaptive and multimodal contractile ring anchoring protein: A simulation study

Graphical abstract



Authors

Aaron R. Hall, Yeol Kyo Choi, Wonpil Im, Dimitrios Vavylonis

Correspondence

vavylonis@lehigh.edu

In brief

Hall et al. used all-atom molecular dynamics simulations to study protein Mid1, which anchors cytokinetic nodes to the plasma membrane during fission yeast cytokinesis. Mid1 diffuses and binds to a yeast-like membrane through its disordered L3 loop. Monomers and dimers can develop additional contacts, indicating its adaptive and multimodal anchoring.

Highlights

- Molecular dynamics simulation of anillin-related Mid1 binding to yeast-like membrane
- Initially unbound C-terminal region establishes contacts through L3 loop of C2 domain
- Evidence for PH domain membrane binding and membrane insertion of NLS region of L3 loop
- Simulations indicate multiple modes of Mid1 binding to membrane as monomer or dimer









Theory

Anillin-related Mid1 as an adaptive and multimodal contractile ring anchoring protein: A simulation study

Aaron R. Hall, Yeol Kyo Choi, Wonpil Im, and Dimitrios Vavylonis 1,3,4,*

- ¹Department of Physics, Lehigh University, Bethlehem, PA 18017, USA
- ²Department of Biological Sciences, Lehigh University, Bethlehem, PA 18017, USA
- ³Center for Computational Biology, Flatiron Institute, New York, NY 10010, USA
- ⁴Lead contact

*Correspondence: vavylonis@lehigh.edu https://doi.org/10.1016/j.str.2023.11.010

SUMMARY

Cytokinesis of animal and fungi cells depends crucially on the anillin scaffold proteins. Fission yeast anillin-related Mid1 anchors cytokinetic ring precursor nodes to the membrane. However, it is unclear if both of its Pleckstrin Homology (PH) and C2 C-terminal domains bind to the membrane as monomers or dimers, and if one domain plays a dominant role. We studied Mid1 membrane binding with all-atom molecular dynamics near a membrane with yeast-like lipid composition. In simulations with the full C terminal region started away from the membrane, Mid1 binds through the disordered L3 loop of C2 in a vertical orientation, with the PH away from the membrane. However, a configuration with both C2 and PH initially bound to the membrane remains associated with the membrane. Simulations of C2-PH dimers show extensive asymmetric membrane contacts. These multiple modes of binding may reflect Mid1's multiple interactions with membranes, node proteins, and ability to sustain mechanical forces.

INTRODUCTION

Cytokinesis, the last step in a cell cycle, is a fundamental biological process in animals and fungi that describes the division of a mother cell into two daughter cells, aided by the formation and contraction of an actomyosin ring. In animal cells, the highly conserved protein anillin is involved in the coordination and localization of cytokinetic ring components and, additionally, anchors the ring to the plasma membrane. ^{1–3} While the N-terminus of anillin is known to bind ring components, its C-terminal region associates to the plasma membrane, through PIP₂ contacts in particular. ⁴ The C-terminal region of anillin is composed of a C2 domain, Pleckstrin Homology (PH) domain, and Rho binding domain (Figures S1A and S1B). The C2 domain contains a nuclear localization sequence (NLS), mutation of which reduces anillin's affinity for the equatorial cortex. ^{5,6}

In model organism *Schizosaccharomyces pombe* (fission yeast), ring positioning is driven by anillin-related protein Mid1,⁷ whose spatial localization in the cell middle is regulated by positive cues, such as nuclear shuttling⁸ and affinity for PIP₂ that is enriched in the cell middle during mitosis,⁹ and negative cues, such as phosphoregulation by the kinase Pom1 that localizes at the cell poles away from the cell middle.¹⁰ At the cell center Mid1 organizes cytokinetic "nodes," primarily consisting of myosin Myo2, formin Cdc12, F-BAR domain containing Cdc15, and IQGAP Rng2.¹¹ Mid1 is an important upstream

component that aids in the recruitment of Myo2 and Cdc15. 12 After a period of node maturation, the medial band of nodes condenses into the cytokinetic ring through Cdc12-driven actin filament elongation and Myo2-driven contraction. 13 Eventually Mid1 leaves the ring prior to its constriction. 14 Membrane connections for both Cdc12 and Myo2 are important in the transmission of force for node movement, although the specifics of the force generation are poorly understood. 15 While Mid1 deletion is not lethal, mid1 \Delta cells form misplaced and tilted cytokinetic rings, which are otherwise tightly regulated to form at the cell center and perpendicular to the long axis of the cell. 16-20 Additionally, cells lacking Mid1 divide slower and at a more variable rate, resulting in cells of more variable length and a higher incidence of multinucleation.²¹ Furthermore, colocalization of important ring components is disrupted and the cytokinetic ring appears to form in a mechanistically dissimilar way to wild-type cells. 19 Super-resolution microscopy studies indicate that Mid1 localizes closer to the membrane than any other node or ring component and therefore understanding the geometry of its membrane binding is critical to understanding the early organization of cytokinetic node and ring components.^{22,23}

Structurally similar to anillin, Mid1 has a C terminal globular region that includes a C2 domain (residues 580–787) connected to a PH domain (805–900, Figures 1A and 1B). While Mid1 lacks the Rho binding domain present in anillin, the geometrical relationship between the PH and C2 domains as studied by





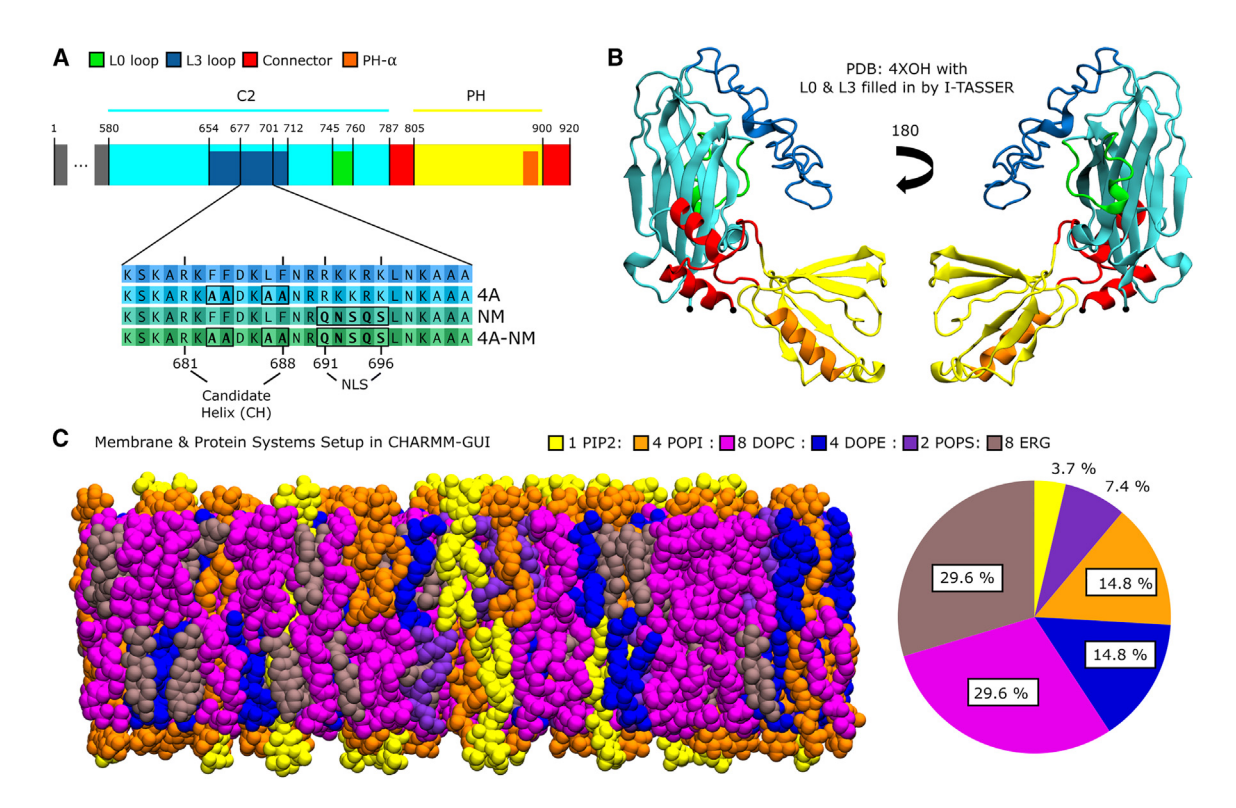


Figure 1. Mid1 protein and membrane system

(A) Mid1 sequence. L3 mutations investigated defined in sequence blowup.

(B) Mid1 structure from PDB: 4XOH⁹ colored as in A. Missing residues that make up the L0 and L3 loop were filled in using I-TASSER.³⁶ Visualization of protein and membrane systems done in VMD.⁵²

(C) Example snapshot of membrane bilayer with composition used in all simulations (left). Legend lists the molar ratio of membrane constituents, also depicted as a pie chart (right), selected to match experimental data.³⁷ Tail saturation was independently matched to experimental data.³⁸ Protein and membrane systems were prepared using CHARMM-GUI (see STAR Methods).

crystallography (for Mid1⁹) and as predicted by AlphaFold^{24,25} are similar (compare Figures S1A and S1B to S1C and S1D), In Mid1, the PH and C2 domains are connected by an intermediate region referred to as a connector (CNCT) domain (787-804, 901-920, Figures 1A and 1B) not present in anillin. The Mid1 C2 domain includes a notably long L3 loop (654-710, Figures 1A and 1B) with a highly negatively charged NLS (691-696, Figure 1A, inset), similar to anillin, near a predicted amphipathic helical structure^{24–26} ("candidate helix", 681–688, Figure 1A, inset), which may localize to the plasma membrane. The structure of the majority of the PH, C2, and CNCT domains (Mid1 C2-PH) has been resolved through X-ray crystallography, excluding the L3 loop and the smaller β 7- β 8 loop ("L0 loop", 745-760, Figures 1A and 1B). In contrast to anillin, Mid1 dimerizes through an interface on its C2 domain, and the structure of a Mid1 C2-PH dimer has been resolved crystallographically (Figures S2A and S2B). Mid1's N-terminus is predicated to be an intrinsically disordered region (IDR, 1-579, Figure 1A, not depicted in Figure 1B) and has been shown to be functionally interchangeable with human anillin's N-terminus.

Both the Mid1 C2 and PH domains have been indicated in membrane binding. Purified Mid1 PH has been shown to bind to negatively charged phosphatidylinositol (PI) lipids, including PIP₂.²⁷ When the PH domain is truncated, Mid1 cortical localization is disrupted in cells lacking Cdr2, a component of medial

interface nodes that precede cytokinetic nodes.²⁷ In addition, mutations to the L3 loop's NLS and candidate helix (CH) have striking effects on the localization of Mid1 during the cell cycle.²⁶ Notably, simulation studies have described the binding of PH and C2 domains of various other proteins to PI lipids.^{28–32}

The orientation of Mid1 when binding the plasma membrane as well as its stoichiometry as a monomer or as a dimer remains unresolved. In the Mid1 C2-PH dimer crystal structure, the L3 loops, one from each C2 domain, are near each other and point in the same direction; in contrast, the PH domains are distant from each other and orient in different directions (Figure S2A). Given the geometry of the dimer in the crystal structure, it is difficult to imagine how the PH domains would bind to the membrane cooperatively with each other or the L3 loops, leading to the hypothesis that the Mid1 dimer membrane binding mode only involves the C2 domain/L3 loops.9 This is consistent with the expected vertical orientation of type II C2 regions, to which Mid1's C2 region belongs.²⁹ However, Mid1 could possibly bind the membrane as either a monomer or as a dimer. Indeed, an orientation for a monomer binding mode using both PH and C2 domains has been hypothesized for both human anillin,9 which is not expected to dimerize, 3,33,34 and Mid1.35

To elucidate how Mid1 binds the membrane, we performed all-atom molecular dynamics (MD) simulations of sections of Mid1 utilizing available structural data, with an experimentally



Table 1. Summary of simulation parameters, to within small fluctuations among replicas				
System Name	System Size (Å)	Number of Total Atoms	Number of Replicas	Total Simulation Time of All Replicas (μs)
C2-PH initialized unbound	145 × 145×200	418,000	10	14.8
L3 segment	91 × 91×152	128,000	10	5.0
L3 segment 4A	89 × 89×156	128,000	10	5.0
L3 segment NM	89 × 89×156	128,000	10	5.0
L3 segment 4A-NM	90 × 90×154	128,000	10	5.0
PH domain	90 × 90×156	128,000	10	5.0
C2-PH initialized unbound 4A	145 × 145×200	418,000	2	3.0
C2-PH initialized unbound NM	145 × 145×200	418,000	2	3.0
C2-PH initialized unbound 4A-NM	145 × 145×200	418,000	2	3.0
C2-PH initialized bound	138 × 138×143	281,000	10	3.3
Candidate Helix in membrane	55 × 55×79	25,000	10	5.0
Candidate Helix 4A in membrane	55 × 55×79	25,000	1	0.3
C2-PH dimer Conformation I	136 × 136×215	409,000	3	1.96
C2-PH dimer Conformation 2	136 × 136×192	366,000	3	1.78

informed membrane representation of the fission yeast plasma membrane near the cell center. Looking at results from Mid1 subdomains in isolation and together, while making comparisons to simulations of known membrane binding defective mutations, provided us with a clearer picture of how the Mid1 monomer and dimer utilizes its various subdomains to make a connection to the fission yeast cortex. These results can further inform our understanding of the Mid1 dimer's role in anchoring the rest of the cytokinetic node to the plasma membrane, as well as more broadly to the function of anillins in cytokinesis.

RESULTS

In order to investigate how the Mid1 protein binds to the membrane, we performed all-atom MD simulations using the crystal structure of the C2-PH domain (PDB: 4X0H)9 with the missing residues filled-in by I-TASSER36 (Figure 1B). Recent studies have characterized the lipid and ergosterol composition of budding yeast, 37 a closely related organism to fission yeast, and the saturation levels of lipid tails in fission yeast membrane.³⁸ We used a lipid bilayer composition that closely matches these data, by independently setting the molar ratio of lipid heads and ergosterol to match the measured ratio 37 and selecting tail saturation levels to match the measured molar ratio.³⁸ The resulting bilayer includes palmitoyl-oleoyl-phospha-(POPIP₂), palmitoyl-oleoyltidylinositol-(4,5)-bisphosphate phosphatidylinositol (POPI), di-oleoyl-phosphatidylethanolamine (DOPE), di-oleoyl-phosphatidylcholine (DOPC), palmitoyl-oleoyl-phosphatidylserine (POPS) and ergosterol (ERG) with molar ratios described in Figure 1C. The upper and lower leaflet compositions are identical, and due to periodic boundaries, molecules can bind freely to either leaflet.

C2-PH binds the membrane quickly through the L3 loop and remains in a vertical configuration with the PH is distal to the membrane

We began by examining if C2-PH can bind to a lipid bilayer with a composition similar to that of fission yeast in isolation when al-

lowed to freely diffuse to the membrane. We created ten initial conditions of the C2-PH started away from the membrane to allow reorientation before binding (Figure S3C). Each simulation had a different rotational orientation, sampled from an approximately uniformly spherical distribution, to study the mode of binding resulting from varying initial conditions, and was run for at least 1,300 ns (Table 1). In all ten simulations, the C2-PH binds initially through the L3 loop (Figure 2A, left, Video S1), which is expected to be flexible and important for Mid1 membrane binding. The L3 loop was continuously associated with the membrane in all cases. The C2 domain remained in a vertical orientation in all cases, though in one simulation, the C2 domain tilted in a way that allowed the L0 loop to make additional contacts and insert into membrane (Figure 2A, third snapshot, Video S2). In this simulation the L0 binding began after 200 ns and persisted until the end of the simulation (1,300 ns). Other simulations lacked L0 contacts or only showed contacts that remained at the surface of the membrane (Video S1, at 250 ns). In 7 out of 10 of the simulations, the molecule bound to the membrane in less than 100 ns (Figure 2B; Videos S1 and S2).

We analyzed membrane contacts, averaged over the ten copies and using the last 1,000 ns for all but one copy which we used the last 700 ns, a period over which the protein bound to the membrane (Figure 2C). The results look nearly identical when only the last 500 ns were used for this analysis (data not shown). L3 binding primarily occurs through interactions with charged POPI and POPIP₂ lipids, especially in the NLS region. However, the CH (residues 681-688) makes notably fewer contacts than surrounding residues. In general membrane insertion of the L3 loop is minimal as quantified by presence of tail contacts. A region of the L3 loop (residues 705-710), also makes strong contacts with charged POPI and POPIP2 lipids, likely due to three positively charged lysines (K706, K708, and K709). The L0 loop contacts mostly involve lipid tails, likely due to its high number of hydrophobic residues (F747, L748, A750, 1751, V753, I755, and I758).

The PH domain did not contact the membrane in any simulations and remained distant to the membrane during L3 binding.

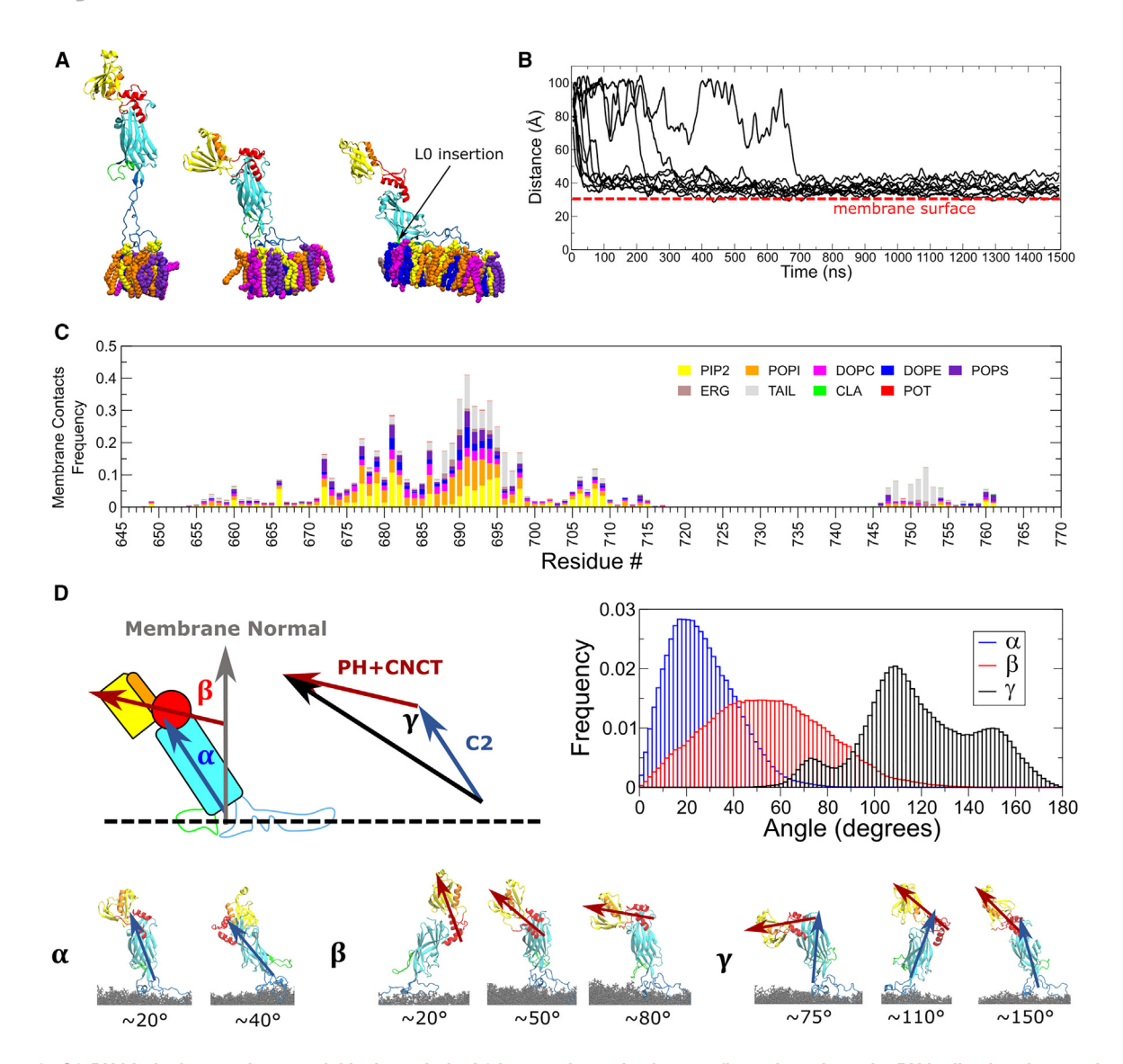


Figure 2. C2-PH binds the membrane quickly through the L3 loop and remains in a configuration where the PH is distal to the membrane (A) Simulation snapshots of Mid1 C2-PH (residues 580–920) binding to the membrane in 3 configurations: through the L3 far from the membrane, through the L3 near to the membrane, and through the L0 and L3. Only showing membrane components within 5 Å. Membrane components are colored according to the legend in (C).

(B) Time sequence of the distance between the L3 and membrane COM along the membrane normal. Data shown is a running average over a 100 ns window. Ten independent simulations were run for at least 1,300 ns with the Mid1 C2-PH started apart from a lipid bilayer of composition described in Figure 1C (see STAR Methods). Red dotted line indicates approximate location of the membrane surface assuming a membrane width of 6 nm.

(C) Contact frequency of C2-PH residues with membrane components. Analysis includes the last 1,000 ns of the ten simulations in (B). Contact frequency is normalized to 1, with the remaining contacts being water (not shown).

(D) Angle frequency (upper right) of defined angles α , β , and γ (upper left) in last 1,000 ns of simulations in (B). Data are normalized and binned in a fixed 100 bins. α is defined as the angle between the first principal component (PC1) of the C2 domain and the membrane normal. β is defined as the angle between PC1 of the PH and connector domain (PH + CNCT) and the membrane normal. γ is defined as the inner angle of a triangle formed by PC1 of C2 and PC1 of PH + CNCT. Simulation snapshots depict representative configurations at the stated angles (bottom).

The C2 domain explores a range of angles with respect to the membrane normal, but this range is not large enough to bring the PH within binding distance to the membrane (Figure 2D). The connector region exhibits noticeable flexibility, which allows the PH domain to explore a wide range of angles with respect to the C2 domain (Figure 2D). However, these fluctuations were also not large enough to bring PH close to the membrane while the L3 loop is bound. Cases with L0 loop binding may cause

some tilt in the C2 domain's binding angle, but this was not enough to allow the PH domain to reach the membrane either (Figure 2D). One explanation for why the PH domain does not bind the membrane in C2-PH initialized unbound simulations could be due to kinetics and geometry: the L3 loop's flexibility may allow it to reach and bind the membrane more quickly than the PH domain, placing the C2-PH region in a vertical orientation with PH far from the membrane.





In summary, the results of Figure 2 show that C2-PH can readily bind the membrane through the L3 loop and reveal a new membrane binding interface of Mid1 in the L0 loop. They indicate geometric and kinetic obstacles for membrane insertion of the CH region and PH binding to the membrane.

Mid1 L3 loop and PH domain can independently bind to the membrane

To further explore membrane binding and insertion of the L3 loop, we first simulated a segment (residues 677-701 in Figure 1A) that includes both the NLS and the CH, which is expected to bind the membrane as an amphipathic helix. We initialized the L3 segment far enough apart from the membrane bilayer to allow it to diffuse before binding (Figure S3A). In all ten independent simulations we performed for 500 ns, the L3 segment bound the membrane quickly (<22 ns, Video S3). Similar to the C2-PH simulations, the binding of the L3 segment occurred primarily through charged lipid contacts with POPIP₂ and POPI (Figure S4A, bottom). Again, we did not observe the expected amphipathic helix binding mode: the hydrophobic residues (F683, F684, L687, and F688) in the CH make very few lipid tail contacts and face mostly away from the membrane (Figure S4B). We thus performed simulations with the CH (residues 681-688) inserted in the membrane. In 10 of 10 simulations the CH migrates from an initial position near the center of the membrane to associate with the lipid heads on either the upper or lower leaflet (Figures S4C and S4D). When we performed a simulation of a CH with mutations to the CH, in which the four hydrophobic residues are replaced by alanines ("4A mutation"), as in a prior experimental study,²⁶ it also associated with the lipid heads of one of the leaflets (Figures S4E and S4F); however, it reached further away from the interior of the lipid membrane than wild type (WT) (Figure S4G). When started helical in these simulations, the CH remained helical throughout (Figure S4H). We conclude that helix formation and membrane insertion of the CH hydrophobic residues is a process that occurs over times longer than μs .

Next, we performed ten independent simulations of the PH domain (residues 805-900, Table 1) initialized far enough apart from the membrane to allow it to freely diffuse (Figure S3B). In all ten simulations, the PH domain was able to quickly bind the membrane (<60 ns, Video S4). However, in eight of the ten simulations, the PH domain bound and remained in contact with terminal residues, which would not be available for binding in the full-length protein. Therefore, we restricted our analysis to PH membrane binding in the two simulations which showed binding independent of the terminal regions (Figure S5A). Similar to the L3 segment, the PH domain makes many contacts with charged POPI and POPIP₂ lipids. Although it appears to form less extensive POPIP₂ contacts, this may be due to insufficient sampling. The binding conformation of the PH domain, with the PH- α distal to the membrane, is similar to other simulations studies of PH domains with the majority of contacts between PIs and the β 1- β 2, β3-β4, β5-β6, and β6-β7 loops. ^{28,30}

Simultaneous C2-PH domain binding is stable

From the C2-PH and PH initialized unbound simulations, we hypothesized that there may be geometric and kinetic barriers that prevent PH binding during the available simulation time either when the C2-PH is away from the membrane, or following L3 binding. In order to investigate if PH binding

might occur over longer times, we initialized the C2-PH such that the L3, L0, and PH domains were in contact with the membrane similar to a proposed configuration³⁵ (Figure 3A, left). We performed ten independent simulations of at least 300 ns for the C2-PH initialized bound configuration and then analyzed the data after the first 100 ns (Table 1). In all ten simulations the PH domain remained bound for the entire duration and showed no signs of detaching (Figure 3A, right, Video S5). The L3, L0, and PH domain formed robust contacts (Figure 3B). The PH domain makes many contacts between lipids, especially POPI, and the β 1- β 2, β 3- β 4, β 5- β 6, and $\beta6-\beta7$ loops. The PH- α remains distal to the membrane as it was initialized. The PH domain contacts seen agree with those when simulated in isolation, including less prevalent contacts with POPIP₂ in comparison to the L3 loop (compare Figure 3B with Figure S5A).

Taken together with the results of the C2-PH initialized unbound simulations, these results indicate that there is a kinetic barrier preventing the PH domain from binding on short timescales, but stable simultaneous binding of C2 and PH domains might occur over long periods. Therefore, the Mid1 C2-PH has several binding interfaces it can utilize to bind stably to the membrane.

L3 mutants can still bind membrane, but NM mutation is weaker

As mutations of the L3 loop have been shown to disrupt Mid1 cortical localization in cells, 26 we were interested in how these mutations would affect membrane binding and contacts. We performed ten simulations each of the L3 segment for a duration of 500 ns under mutations to the CH, in which four residues are replaced by alanines (4A, Video S6), mutations to the NLS, in which five positively charged residues are replaced with the sequence QNSQS (NLS mutant, NM, Video S7), and a double mutant of these mutations (4A-NM, Video S8), as in a prior study²⁶ (Figure 1A and Table 1). The first 100 ns were excluded from the analysis by which time the L3 segment had bound the membrane in all simulations. None of the mutations resulted in completely preventing membrane binding of the L3 segment in any of the simulations. The helix propensity of the CH 681-688 remained similarly weak to WT for the 4A mutation and was even lower for the NM and 4A-NM mutations (Figure 4A). The membrane contacts of the 4A mutant are not qualitatively distinguishable from WT. However, the NM and 4A-NM mutants have noticeably less contacts with POPI and POPIP2 in the NLS region (compare Figure S6 with Figure S4A).

We additionally performed two simulations for each mutation of the whole C2-PH in two different rotational orientations started apart from the membrane for a duration of 1,500 ns (Table 1). In the 4A simulations, the C2-PH quickly bound the membrane through the L3 loop on timescales similar to that of WT simulations (Figure 4B). In one of the NM simulations it took longer than 1,000 ns for the C2-PH to bind through the L3 loop, while in the other simulation it made several membrane approaches before binding (Figure 4B). While in one 4A-NM simulation, the C2-PH bound on timescales similar to WT, in the other simulation it failed to bind during the entire 1,500 ns duration (Figure 4B). The membrane contacts within the 677–701 region of the 4A



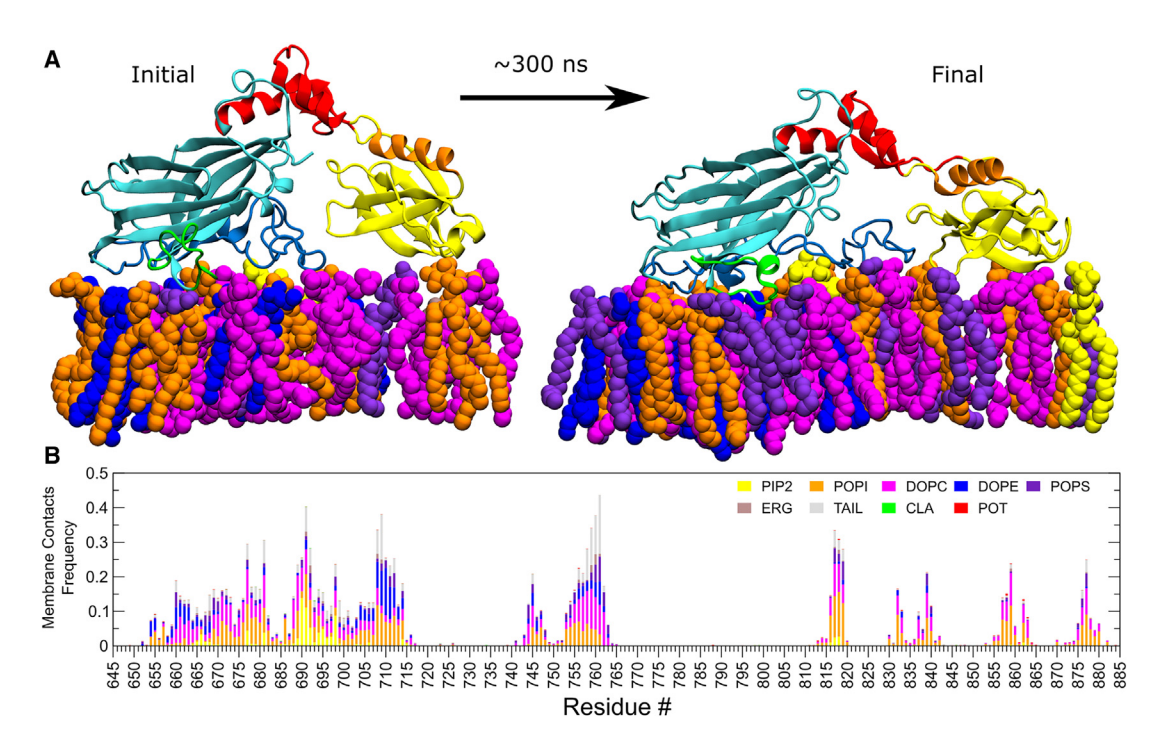


Figure 3. Simultaneous C2-PH domain binding is stable

(A) The Mid1 C2-PH (residues 580–920) was initialized near the membrane in a configuration similar to that proposed in.³⁵ After equilibration, 10 independent simulations were performed for at least 300 ns (see STAR Methods). Snapshots show the initial and final configuration of one simulation. Only showing membrane components within 5 Å. Membrane components are colored according to the legend in (B).

(B) Contact frequency of the ten independent simulations. The first 100 ns from each simulation were ignored. Contact frequency is normalized to 1, with the remaining contacts being water (not shown).

simulations appear less robust compared to WT, though additional contacts are formed with greater frequency in the 658–663 region of the L3 loop (Figure 4C, compare to Figure 2C). Both the NM and 4A-NM mutations formed drastically fewer contacts with less frequency in comparison to WT (Figure 4C, compare to Figure 2C). Interestingly, during the NM and 4A-NM simulations where the L3 loop remained unbound for an extended duration (>1 μ s), the PH domain also failed to bind, further ruling out PH binding on the timescales available during these simulations.

The results of Figure 4 show that mutation of the NLS (NM) or of both NLS and CH (4A-NM) slow down and weaken association to the studied plasma membrane, in agreement with experiments. However, we did not observe statistically significant effects of 4A mutations. The latter mutation may influence membrane insertion of this region, a process we argued is occurring on longer timescales to our simulations. In all cases, the L3 loop can make robust contacts on short timescales such that the studied mutations do not outright prevent membrane association.

Mid1 dimer forms extensive asymmetric membrane contacts

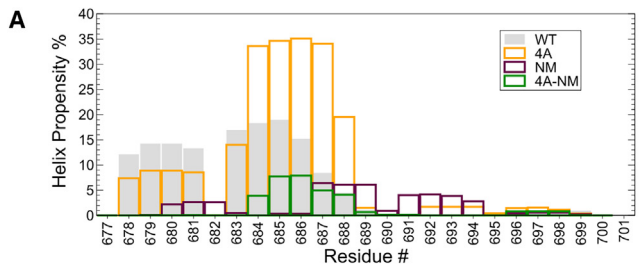
In order to investigate Mid1 dimer binding modes in a computational feasible way, we aligned the crystallographic Mid1 dimer⁹ at the C2 dimerization interface (Figure S2B) with structures of a simulated membrane-bound Mid1 monomer. We thus created two initial dimer conformations: "Conformation 1" (Figure 5A),

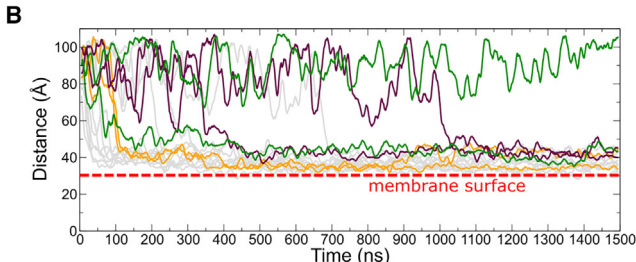
where one C2-PH is bound through the L3 loop only, obtained near the end of a C2-PH initialized unbound simulation (Figure 2), and "Conformation 2" (Figure 5C) where one C2-PH is bound to the membrane through both L2 and PH, obtained near the end of a C2-PH initialized bound simulation (Figure 3). For both initial dimer conformations, the aligned added monomer did not have any membrane contacts and we run three replicas for at least 480 ns for each conformation.

For both initial conformations, the dimerization through C2 remained stable and we observed an overall increase of membrane contacts during the simulations utilizing the L3, L0, and PH binding interfaces (Figure 5). In all Conformation 1 replicas, the initially bound monomer retained L3 loop contacts and further developed some L0 contacts, while the PH domain remained distant to the membrane (Figure 5B). The added monomer in Conformation 1 established L3 loop membrane contacts that included the CH and NLS regions; its PH domain came closer to the membrane and established contacts mainly through residues 800-815, in an upside-down orientation with the PH-α close to the membrane (Figure 5B and Video S9). A similar behavior was seen in all replicas of Conformation 2 where the initially bound monomer retained its L3, L0, and PH membrane contacts (Figure 5D). In the added monomer in Conformation 2 the L3 loop started father from the membrane, establishing somewhat less extended L3 loop contacts that contained the CH and NLS region; the PH domain also established contacts with residues 810-816 in an upside-down orientation as in Conformation 1 (Figures 5D and Video S10). The results of the simulations









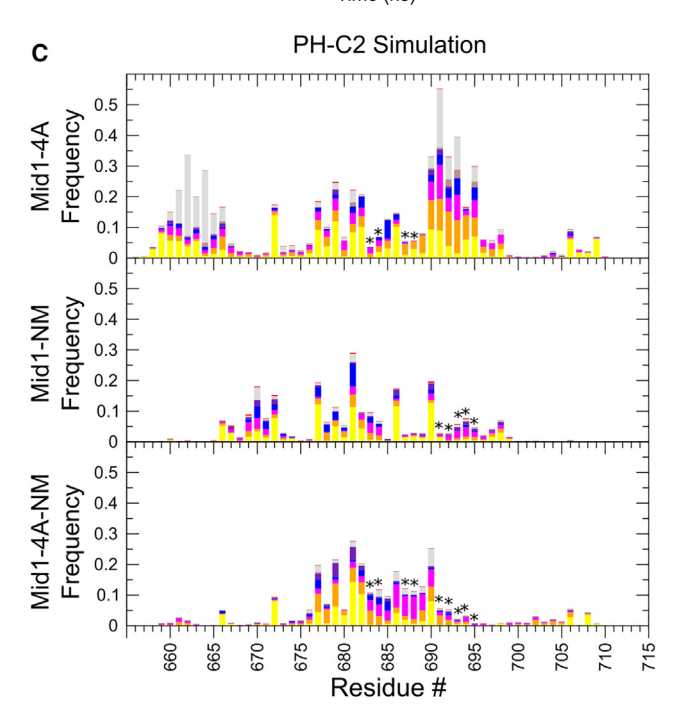


Figure 4. L3 mutants can still bind membrane, but NLS mutation is weaker

(A) Ten 500 ns simulations were performed of the L3 segment (residues 677-701) for each mutation defined in Figure 1A. The first 100 ns of each simulation were not included in analysis. Helix propensity was calculated as in Figure 2A. (B) Time sequence of the distance between the L3 and membrane COM along the membrane normal. Comparison of two simulations performed for each mutation with the Mid1 C2-PH (residues 580-920) for 1,500 ns to unmutated simulations of Figure 2B. Data shown is a running average over a 100 ns window.

(C) Contact frequency between L3 segment residues for C2-PH mutants. Asterisks mark mutated residues. Contact frequency analysis was performed on the last 1,000 ns except for two simulations: one 4A-NM simulation which never bound and one NM simulation which did not bind until late into the simulation. No contacts were calculated for the unbound 4A-NM simulation. Contacts were calculated for the last 400 ns for the late binding NM simulation in which it was bound. All contact frequency plots are normalized to 1, with the remaining contacts being water (not shown).

of Figure 5 lead us to conclude that the Mid1 dimer can utilize the L0, L3, and PH binding interfaces to bind the membrane in an asymmetric and multimodal fashion.

DISCUSSION

Our results (Figures 2, 3, 4, and 5) show that Mid1 monomers and dimers have many modes of membrane binding, which may reflect their multiple interactions with membranes and other cytokinetic ring proteins. Figure 6 shows a model of Mid1 in nodes, which takes into consideration super-resolution data of node proteins²² (slightly shifted by 10 nm to place Mid1 adjacent to the plasma membrane), as well as the estimated size of Mid1's IDR region based on coarse-grained MD simulations.³⁹ This figure indicates how a membrane layer of \sim 8-10 Mid1 per node^{22,40} provides a scaffolding layer for node proteins, together with about twice as many membrane-bound Cdc15 and Rng2,39 as well as Cdr2 (not shown), thus helping anchor formin Cdc12 and type II myosin Myo2 (Figure S7). The multiple modes of Mid1 membrane binding may reflect its ability to sustain mechanical forces as Myo2 pulls on Cdc12-nucleated actin filaments, leading to the condensation of the band of nodes into a ring through the opposing steric hindrance by membrane-associated ER.41 These membrane attachments should also control the resistance of node movement to applied force, an important biophysical parameter for cytokinetic ring organization. Recent evidence suggests that IDR regions of Cdc15 promote condensation of Cdc15 through forces related to liquid-liquid phase separation.³⁹ Flexibility in Mid1 membrane binding may thus also be related to its ability to participate into a disordered condensate through its IDR region, which is of comparable size to Cdc15.

In our simulations, the Mid1 monomer initially binds through the L3 loop (Figures 6 I and 6 II), but can further bind through the L0 loop (Figure 6 III) and PH domain (Figure 6B IV). The binding we observe through the L3 loop is fast and primarily driven by positively charged residues making contacts with negatively charge PI lipids, particularly in the NLS and with POPIP2. However, mutation of the NLS alone is not sufficient to prevent L3 loop association to the membrane in our simulations, with neighboring regions still able to make contacts. Residues in the CH region of the L3 loop made membrane contacts, though these were less noticeable compared to the NLS region; correspondingly, we did not see a large effect from mutations to the CH, which have been shown to cause Mid1 to be largely cytoplasmic in experiment.²⁶ However, the CH region remained helical and embedded in the membrane when initialized inside the membrane. We conclude that Mid1 stabilization on the membrane through helix formation and membrane insertion of hydrophobic or aromatic residues occurs over timescales beyond the reach of serial MD simulations, as has been the case for simulations with liquid-ordered membranes.42 The L0 loop contacts, which we observed less often in C2-PH initialized unbound simulations, but appear stable after formation, include hydrophobic residues that insert into the membrane. While we could not observe the PH domain contacting the membrane in C2-PH initialized unbound simulations, the PH domain remains stably bound when started in contact. Overall, these results indicate that short timescale binding of the L3 loop, in particular the NLS, drives the



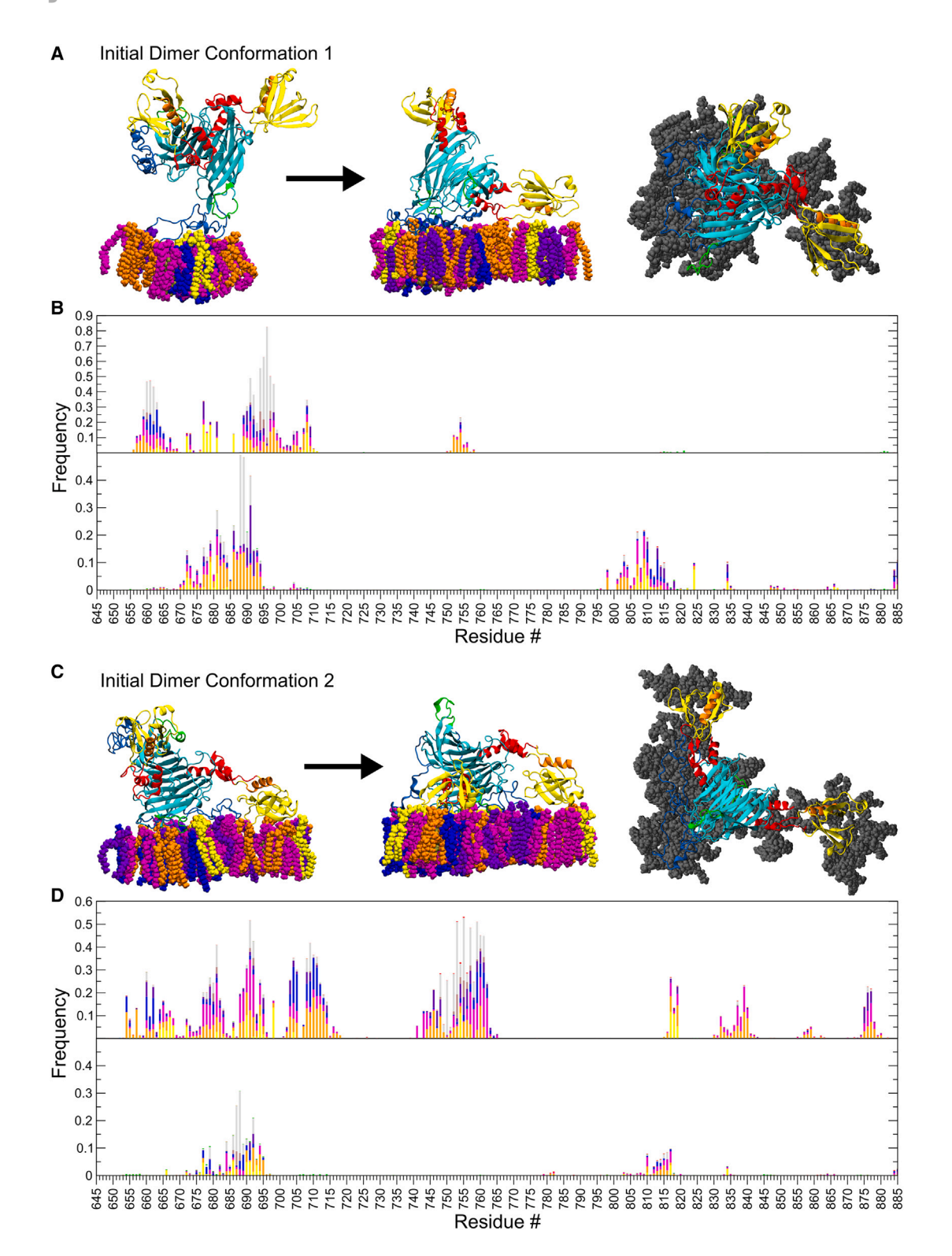


Figure 5. C2-PH dimer binds asymmetrically to membrane

(A) Initial and final snapshots of C2-PH dimer in Conformation 1 with one member initially bound to membrane through C2 domain, from representative replica. Top final snapshot view shows contacted lipids in gray. Three replicas run for at least 480 ns.

- (B) Membrane contacts. Top: monomer initially bound to membrane; bottom: added monomer. At least the first 100 ns excluded from analysis.
- (C) Same as (A) but with one member of C2-PH dimer initially bound to the membrane through both C2 and PH domains (representative replica).
- (D) Membrane contacts as (B), for simulations of (C).



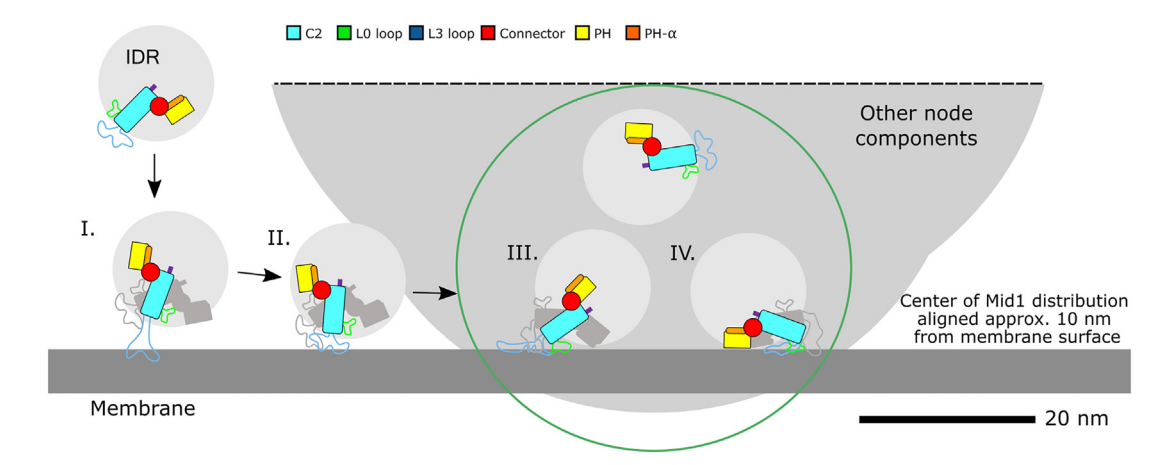


Figure 6. Proposed Mid1 binding to cytokinetic nodes

Zoom in on node membrane proximal region with zone of Mid1 distribution (green line) shifted vertically by 10 nm from experiments²² such that the center of the Mid1 distribution is approximately 10 nm from the surface of the membrane; this is the approximate distance of the connector region from the membrane when the L3 loop binds in an extended way. Membrane shown 5 nm thick. Mid1's flexible N-terminal IDR region shown in light gray, with C2 attachment point in purple. Mid1 binds initially through the L3 loop and can dimerize using its C2 interface (I). Collapsing further onto the membrane either as a monomer or dimer, Mid1 can form additional contacts in its L3 loop (II), L0 loop (III), or PH domain (IV). In a dimer, the second monomer can bind in an asymmetric orientation with its L3 loop and PH domain in an upside-down configuration.

Mid1 protein's affinity for PIP₂ lipids near the center of fission yeast, but that long timescale binding requires making more stable interactions such as those through the L0 loop, PH domain, and CH membrane insertion.

Another way Mid1 strengthens its membrane affinity is through dimerization. When a second monomer was added to simulations of Mid1 monomer bound to the membrane in two different conformations, the dimerization through the C2 domain remained stable, the membrane contacts of the initially bound monomer were not perturbed, and the added dimer developed an increasing number of membrane contacts through its L3 loop and PH domain. Interestingly, in both conformations, the PH domain of the added dimer bound upside-down when compared to the canonical PH domain membrane binding orientation. In one of two conformations the PH domain of initially bound monomer remained distal to the membrane.

This begs the question as to the role of the PH domains distal to the membrane. Although binding of PH domains to PI lipids is well studied, PH domains also mediate protein-protein interactions. 43,44 For example, human anillin, drosophila anillin, and Mid2 PH are known to recruit septins. 45-48 However, little is known about Mid1 PH's possible role in protein-protein interactions, but it has been suggested it may directly or indirectly interact with ESCRT-associated protein Vps4.49 The Mid1 PH domain's preference for negatively charged PI lipids may indicate a potential role in regulation by phosphorylation, which adds a negatively charged phosphate group to an amino acid. Mid1 is known to be heavily phosphorylated on its N-terminal IDR, 7,35 and regulation by phosphorylation is a common feature of other node proteins. 39,50,51 However, what potential role the PH domain would play in regulation via phosphorylation has not been explored.

In conclusion, this study highlights the multiple binding modes available to Mid1 monomers and dimers, with the implications of the results including Mid1 localization in the cell, Mid1 regulation,

and interfaces available to Mid1 binding partners. Even though our results focused on fission yeast Mid1, they should be relevant for anillin family members more broadly. Fission yeast Mid2, which also plays a stabilizing role for the contractile ring, is predicted by AlphaFold to have a similar geometrical arrangement of C2-PH to that of Mid1's C2-PH, with most obvious differences in the CNCT, L3, L0, and PH lipid binding regions (compare Figure S1C to S1E). AlphaFold structures of Mid1 and Mid2 of the related medially dividing *S. japonicus* bear close resemblance to the corresponding structures of *S. pombe* (compare Figure S1C to S1D and S1E to S1F). Apart from the extra Rho binding region adjacent to C2, AlphaFold predicted structures of drosophila and human anillin share a similar structure and apparent membrane binding interfaces to those of Mid1 (compare Figures S1A and S1B to S1C).

STAR*METHODS

Detailed methods are provided in the online version of this paper and include the following:

- KEY RESOURCES TABLE
- RESOURCE AVAILABILITY
 - Lead contact
 - Materials availability
 - O Data and code availability
- METHOD DETAILS
 - Systems
 - MD simulations
- QUANTIFICATION AND STATISTICAL ANALYSIS

SUPPLEMENTAL INFORMATION

Supplemental information can be found online at https://doi.org/10.1016/j.str. 2023.11.010.

Structure

Theory



ACKNOWLEDGMENTS

We thank Jian-Qiu Wu, Aurelia Honerkamp-Smith, and Thomas Pollard for feedback and suggestions. This work was supported by NIH grant R35GM136372 to D.V. and by NSF grant MCB-2111728 to W.I. This research used resources of the Argonne Leadership Computing Facility, which is a DOE Office of Science User Facility supported under Contract DE-AC02-06CH11357. Portions of this research were conducted on Lehigh University's Research Computing infrastructure partially supported by NSF Award 2019035 and the high-performance computing capabilities of the Extreme Science and Engineering Discovery Environment (XSEDE) and Advanced Cyberinfrastructure Coordination Ecosystem: Services & Support (ACCESS), supported by the National Science Foundation, project no. MCB180021.

AUTHOR CONTRIBUTIONS

A.R.H. performed computer simulations and analyzed data, with input from Y.K.C., W.I., and D.V. A.R.H., Y.K.C., W.I., and D.V. designed research and wrote the paper.

DECLARATION OF INTERESTS

The authors declare no competing interests.

Received: February 6, 2023 Revised: October 13, 2023 Accepted: November 21, 2023 Published: December 15, 2023

REFERENCES

- 1. Hickson, G.R.X., and O'Farrell, P.H. (2008). Anillin: a pivotal organizer of the cytokinetic machinery. Biochem. Soc. Trans. *36*, 439–441.
- D'Avino, P.P. (2009). How to scaffold the contractile ring for a safe cytokinesis lessons from Anillin-related proteins. J. Cell Sci. 122, 1071–1079.
- 3. Piekny, A.J., and Maddox, A.S. (2010). The myriad roles of Anillin during cytokinesis. Semin. Cell Dev. Biol. *21*, 881–891.
- Liu, J., Fairn, G.D., Ceccarelli, D.F., Sicheri, F., and Wilde, A. (2012).
 Cleavage Furrow Organization Requires PIP2-Mediated Recruitment of Anillin. Curr. Biol. 22, 64–69.
- Nguyen, L.T.S., and Robinson, D.N. (2020). The Unusual Suspects in Cytokinesis: Fitting the Pieces Together. Front. Cell Dev. Biol. 8, 441.
- Beaudet, D., Akhshi, T., Phillipp, J., Law, C., and Piekny, A. (2017). Active Ran regulates anillin function during cytokinesis. Mol. Biol. Cell 28, 3517–3531
- Rezig, I.M., Yaduma, W.G., Gould, G.W., and McInerny, C.J. (2023). The role of anillin/Mid1p during medial division and cytokinesis: from fission yeast to cancer cells. Cell Cycle 22, 633–644.
- 8. Paoletti, A., and Chang, F. (2000). Analysis of mid1p, a protein required for placement of the cell division site, reveals a link between the nucleus and the cell surface in fission yeast. Mol. Biol. Cell 11, 2757–2773.
- Sun, L., Guan, R., Lee, I.J., Liu, Y., Chen, M., Wang, J., Wu, J.Q., and Chen, Z. (2015). Mechanistic insights into the anchorage of the contractile ring by anillin and Mid1. Dev. Cell 33, 413–426.
- Bähler, J., Steever, A.B., Wheatley, S., Wang, Y.I., Pringle, J.R., Gould, K.L., and McCollum, D. (1998). Role of polo kinase and Mid1p in determining the site of cell division in fission yeast. J. Cell Biol. 143, 1603–1616.
- Pollard, T.D., and Wu, J.-Q. (2010). Understanding cytokinesis: lessons from fission yeast. Nature reviews 11, 149–155.
- Laporte, D., Coffman, V.C., Lee, I.J., and Wu, J.Q. (2011). Assembly and architecture of precursor nodes during fission yeast cytokinesis. J. Cell Biol. 192, 1005–1021.
- Vavylonis, D., Wu, J.Q., Hao, S., O'Shaughnessy, B., and Pollard, T.D. (2008). Assembly mechanism of the contractile ring for cytokinesis by fission yeast. Science 319, 97–100.

- Willet, A.H., DeWitt, A.K., Beckley, J.R., Clifford, D.M., and Gould, K.L. (2019). NDR Kinase Sid2 Drives Anillin-like Mid1 from the Membrane to Promote Cytokinesis and Medial Division Site Placement. Curr. Biol. 29, 1055–1063.e2.
- Pollard, T.D., and O'Shaughnessy, B. (2019). Molecular Mechanism of Cytokinesis. Annu. Rev. Biochem. 88, 661–689.
- Chang, F., Woollard, A., and Nurse, P. (1996). Isolation and characterization of fission yeast mutants defective in the assembly and placement of the contractile actin ring. J. Cell Sci. 109, 131–142.
- Sohrmann, M., Fankhauser, C., Brodbeck, C., and Simanis, V. (1996). The dmf1/mid1 gene is essential for correct positioning of the division septum in fission yeast. Genes Dev. 10, 2707–2719.
- Huang, Y., Yan, H., and Balasubramanian, M.K. (2008). Assembly of normal actomyosin rings in the absence of Mid1p and cortical nodes in fission yeast. J. Cell Biol. 183, 979–988.
- Saha, S., and Pollard, T.D. (2012). Anillin-related protein Mid1p coordinates the assembly of the cytokinetic contractile ring in fission yeast. Mol. Biol. Cell 23, 3982–3992.
- Saha, S., and Pollard, T.D. (2012). Characterization of structural and functional domains of the anillin-related protein Mid1p that contribute to cytokinesis in fission yeast. Mol. Biol. Cell 23, 3993–4007.
- Hachet, O., and Simanis, V. (2008). Mid1p/anillin and the septation initiation network orchestrate contractile ring assembly for cytokinesis. Genes Dev. 22, 3205–3216.
- Laplante, C., Huang, F., Tebbs, I.R., Bewersdorf, J., and Pollard, T.D. (2016). Molecular organization of cytokinesis nodes and contractile rings by super-resolution fluorescence microscopy of live fission yeast. USA 113. E5876–E5885.
- McDonald, N.A., Lind, A.L., Smith, S.E., Li, R., and Gould, K.L. (2017).
 Nanoscale architecture of the Schizosaccharomyces pombe contractile ring. Elife 6, e28865.
- Jumper, J., Evans, R., Pritzel, A., Green, T., Figurnov, M., Ronneberger, O., Tunyasuvunakool, K., Bates, R., Žídek, A., Potapenko, A., et al. (2021). Highly accurate protein structure prediction with AlphaFold. Nature 596, 583–589.
- 25. Varadi, M., Anyango, S., Deshpande, M., Nair, S., Natassia, C., Yordanova, G., Yuan, D., Stroe, O., Wood, G., Laydon, A., et al. (2022). AlphaFold Protein Structure Database: massively expanding the structural coverage of protein-sequence space with high-accuracy models. Nucleic Acids Res. 50, D439–D444.
- Celton-Morizur, S., Bordes, N., Fraisier, V., Tran, P.T., and Paoletti, A. (2004). C-terminal anchoring of mid1p to membranes stabilizes cytokinetic ring position in early mitosis in fission yeast. Mol. Cell Biol. 24, 10621–10635.
- Lee, I.J., and Wu, J.-Q. (2012). Characterization of Mid1 domains for targeting and scaffolding in fission yeast cytokinesis. J. Cell Sci. 125, 2973–2985.
- Aleshin, A.E., Yao, Y., Iftikhar, A., Bobkov, A.A., Yu, J., Cadwell, G., Klein, M.G., Dong, C., Bankston, L.A., Liddington, R.C., et al. (2021). Structural basis for the association of PLEKHA7 with membrane-embedded phosphatidylinositol lipids. Structure 29, 1029–1039.e3.
- Larsen, A.H., and Sansom, M.S.P. (2021). Binding of Ca²⁺-independent C2 domains to lipid membranes: A multi-scale molecular dynamics study. Structure 29, 1200–1213.e2.
- Le Huray, K.I.P., Wang, H., Sobott, F., and Kalli, A.C. (2022). Systematic simulation of the interactions of pleckstrin homology domains with membranes. Sci. Adv. 8, eabn6992.
- Alnaas, A.A., Watson-Siriboe, A., Tran, S., Negussie, M., Henderson, J.A., Osterberg, J.R., Chon, N.L., Harrott, B.M., Oviedo, J., Lyakhova, T., et al. (2021). Multivalent lipid targeting by the calcium-independent C2A domain of synaptotagmin-like protein 4/granuphilin. J. Biol. Chem. 296, 100159.
- Pant, S., and Tajkhorshid, E. (2020). Microscopic Characterization of GRP1 PH Domain Interaction with Anionic Membranes. J. Comput. Chem. 41, 489–499.





- 33. Matsuda, K., Sugawa, M., Yamagishi, M., Kodera, N., and Yajima, J. (2020). Visualizing dynamic actin cross-linking processes driven by the actin-binding protein anillin. FEBS Lett. 594, 1237-1247.
- 34. Jananji, S., Risi, C., Lindamulage, I.K.S., Picard, L.-P., Van Sciver, R., Laflamme, G., Albaghjati, A., Hickson, G.R.X., Kwok, B.H., and Galkin, V.E. (2017). Multimodal and Polymorphic Interactions between Anillin and Actin: Their Implications for Cytokinesis. J. Mol. Biol. 429, 715-731.
- 35. Chatterjee, M., and Pollard, T.D. (2019). The Functionally Important N-Terminal Half of Fission Yeast Mid1p Anillin Is Intrinsically Disordered and Undergoes Phase Separation. Biochemistry 58, 3031-3041.
- 36. Yang, J., and Zhang, Y. (2015). I-TASSER server: new development for protein structure and function predictions. Nucleic Acids Res. 43, W174-W181.
- 37. van 't Klooster, J.S., Cheng, T.-Y., Sikkema, H.R., Jeucken, A., Moody, B., and Poolman, B. (2020). Periprotein lipidomes of Saccharomyces cerevisiae provide a flexible environment for conformational changes of membrane proteins. Elife 9, e57003.
- 38. Makarova, M., Peter, M., Balogh, G., Glatz, A., MacRae, J.I., Lopez Mora, N., Booth, P., Makeyev, E., Vigh, L., and Oliferenko, S. (2020). Delineating the Rules for Structural Adaptation of Membrane-Associated Proteins to Evolutionary Changes in Membrane Lipidome. Curr. Biol. 30, 367-380.e8.
- 39. Bhattacharjee, R., Hall, A.R., Mangione, M.C., Igarashi, M.G., Roberts-Galbraith, R.H., Chen, J.-S., Vavylonis, D., and Gould, K.L. (2023). Multiple polarity kinases inhibit phase separation of F-BAR protein Cdc15 and antagonize cytokinetic ring assembly in fission yeast. Elife
- 40. Sayyad, W.A., and Pollard, T.D. (2022). The number of cytokinesis nodes in mitotic fission yeast scales with cell size. Elife 11, e76249.
- 41. Zhang, D., Bidone, T.C., and Vavylonis, D. (2016). ER-PM Contacts Define Actomyosin Kinetics for Proper Contractile Ring Assembly. Curr. Biol. 26, 647-653.
- 42. Muller, M.P., Jiang, T., Sun, C., Lihan, M., Pant, S., Mahinthichaichan, P., Trifan, A., and Tajkhorshid, E. (2019). Characterization of Lipid-Protein Interactions and Lipid-Mediated Modulation of Membrane Protein Function through Molecular Simulation. Chem. Rev. 119, 6086-6161.
- 43. Lenoir, M., Kufareva, I., Abagyan, R., and Overduin, M. (2015). Membrane and Protein Interactions of the Pleckstrin Homology Domain Superfamily. Membranes 5, 646-663.
- 44. Scheffzek, K., and Welti, S. (2012). Pleckstrin homology (PH) like domains versatile modules in protein-protein interaction platforms. FEBS Lett. 586, 2662-2673.
- 45. Kinoshita, M., Field, C.M., Coughlin, M.L., Straight, A.F., and Mitchison, T.J. (2002). Self- and Actin-Templated Assembly of Mammalian Septins. Dev. Cell 3, 791-802.
- 46. Oegema, K., Savoian, M.S., Mitchison, T.J., and Field, C.M. (2000). Functional Analysis of a Human Homologue of the Drosophila Actin Binding Protein Anillin Suggests a Role in Cytokinesis. J. Cell Biol. 150,
- 47. Berlin, A., Paoletti, A., and Chang, F. (2003). Mid2p stabilizes septin rings during cytokinesis in fission yeast. J. Cell Biol. 160, 1083-1092.
- 48. Tasto, J.J., Morrell, J.L., and Gould, K.L. (2003). An anillin homologue, Mid2p, acts during fission yeast cytokinesis to organize the septin ring and promote cell separation. J. Cell Biol. 160, 1093-1103.
- 49. Rezig, I.M., Yaduma, W.G., Gould, G.W., and McInerny, C.J. (2021). Anillin/Mid1p interacts with the ESCRT-associated protein Vps4p and mitotic kinases to regulate cytokinesis in fission yeast. Cell Cycle 20, 1845-1860.
- 50. Bhattacharjee, R., Mangione, M.C., Wos, M., Chen, J.-S., Snider, C.E., Roberts-Galbraith, R.H., McDonald, N.A., Presti, L.L., Martin, S.G., and

- Gould, K.L. (2020). DYRK kinase Pom1 drives F-BAR protein Cdc15 from the membrane to promote medial division. Mol. Biol. Cell 31, 917-929.
- 51. Rincon, S.A., Bhatia, P., Bicho, C., Guzman-Vendrell, M., Fraisier, V., Borek, W.E., Alves, F.d.L., Dingli, F., Loew, D., Rappsilber, J., et al. (2014). Pom1 regulates the assembly of Cdr2-Mid1 cortical nodes for robust spatial control of cytokinesis. J. Cell Biol. 206, 61-77.
- 52. Humphrey, W., Dalke, A., and Schulten, K. (1996). VMD: Visual molecular dynamics. J. Mol. Graph. 14, 33-38.
- 53. Jo, S., Kim, T., Iyer, V.G., and Im, W. (2008). CHARMM-GUI: A web-based graphical user interface for CHARMM. J. Comput. Chem. 29, 1859-1865.
- 54. Wu, E.L., Cheng, X., Jo, S., Rui, H., Song, K.C., Dávila-Contreras, E.M., Qi, Y., Lee, J., Monje-Galvan, V., Venable, R.M., et al. (2014). CHARMM-GUI Membrane Builder toward realistic biological membrane simulations. J. Comput. Chem. 35, 1997-2004.
- 55. Jo, S., Lim, J.B., Klauda, J.B., and Im, W. (2009). CHARMM-GUI Membrane Builder for Mixed Bilayers and Its Application to Yeast Membranes. Biophys. J. 97, 50-58.
- 56. Jo, S., Kim, T., and Im, W. (2007). Automated Builder and Database of Protein/Membrane Complexes for Molecular Dynamics Simulations. PLoS One 2, e880.
- 57. Lee, J., Patel, D.S., Ståhle, J., Park, S.-J., Kern, N.R., Kim, S., Lee, J., Cheng, X., Valvano, M.A., Holst, O., et al. (2019). CHARMM-GUI Membrane Builder for Complex Biological Membrane Simulations with Glycolipids and Lipoglycans. J. Chem. Theory Comput. 15, 775-786.
- 58. Brooks, B.R., Brooks, C.L., Iii, Mackerell, A.D., Jr., Nilsson, L., Petrella, R.J., Roux, B., Won, Y., Archontis, G., Bartels, C., Boresch, S., et al. (2009). CHARMM: The biomolecular simulation program. J. Comput. Chem. 30, 1545-1614.
- 59. Lee, J., Cheng, X., Swails, J.M., Yeom, M.S., Eastman, P.K., Lemkul, J.A., Wei, S., Buckner, J., Jeong, J.C., Qi, Y., et al. (2016). CHARMM-GUI Input Generator for NAMD, GROMACS, AMBER, OpenMM, and CHARMM/ OpenMM Simulations Using the CHARMM36 Additive Force Field. J. Chem. Theory Comput. 12, 405-413.
- 60. Klauda, J.B., Venable, R.M., Freites, J.A., O'Connor, J.W., Tobias, D.J., Mondragon-Ramirez, C., Vorobyov, I., MacKerell, A.D., Jr., and Pastor, R.W. (2010). Update of the CHARMM All-Atom Additive Force Field for Lipids: Validation on Six Lipid Types. J. Phys. Chem. B 114, 7830-7843.
- 61. Abraham, M.J., Murtola, T., Schulz, R., Páll, S., Smith, J.C., Hess, B., and Lindahl, E. (2015). GROMACS: High performance molecular simulations through multi-level parallelism from laptops to supercomputers. SoftwareX 1-2, 19-25.
- 62. Jorgensen, W.L., Chandrasekhar, J., Madura, J.D., Impey, R.W., and Klein, M.L. (1983). Comparison of simple potential functions for simulating liquid water. J. Chem. Phys. 79, 926-935.
- 63. Gao, Y., Lee, J., Smith, I.P.S., Lee, H., Kim, S., Qi, Y., Klauda, J.B., Widmalm, G., Khalid, S., and Im, W. (2021). CHARMM-GUI Supports Hydrogen Mass Repartitioning and Different Protonation States of Phosphates in Lipopolysaccharides. J. Chem. Inf. Model. 61, 831–839.
- 64. McGibbon, R.T., Beauchamp, K.A., Harrigan, M.P., Klein, C., Swails, J.M., Hernández, C.X., Schwantes, C.R., Wang, L.-P., Lane, T.J., and Pande, V.S. (2015). MDTraj: A Modern Open Library for the Analysis of Molecular Dynamics Trajectories. Biophys. J. 109, 1528-1532.
- 65. Touw, W.G., Baakman, C., Black, J., te Beek, T.A.H., Krieger, E., Joosten, R.P., and Vriend, G. (2015). A series of PDB-related databanks for everyday needs. Nucleic Acids Res. 43, D364-D368.
- 66. Kabsch, W., and Sander, C. (1983). Dictionary of protein secondary structure: Pattern recognition of hydrogen-bonded and geometrical features. Biopolymers 22, 2577-2637.

Structure





STAR*METHODS

KEY RESOURCES TABLE

REAGENT or RESOURCE	SOURCE	IDENTIFIER	
Deposited data			
Molecular dynamics initialization files to reproduce the simulations reported in this paper	This work	https://zenodo.org/records/10072308 https://doi.org/10.5281/zenodo.10072308	
Software and algorithms			
I-TASSER	Sun et al., 2015 ⁹	https://zhanggroup.org/I-TASSER/	
CHARMM-GUI	Jo et al., 2007 ⁵⁶ ; Jo et al., 2008 ⁵³ ; Jo et al., 2009 ⁵⁵ ; Lee et al., 2019 ⁵⁷ ; Wu et al., 2014 ⁵⁴	https://www.charmm-gui.org/	
GROMACS versions 2018.5 and 2020.4	Brooks et al., 2009 ⁵⁸ ; Lee et al., 2016 ⁵⁹ ; Abraham et al., 2015 ⁶¹	https://www.gromacs.org/	
CHARMM36(m)	Brooks et al., 2009 ⁵⁸ ; Klauda et al., 2010 ⁶⁰	https://www.charmm.org/	
VMD	Humphrey et al., 1996 ⁵²	https://www.ks.uiuc.edu/Research/vmd/	
MDTraj	McGibbon et al., 2015 ⁶⁴	https://www.mdtraj.org/	
DSSP	Kabsch and Sander, 1983 ⁶⁶ ; Touw et al., 2015 ⁶⁵	https://pdb-redo.eu/dssp	

RESOURCE AVAILABILITY

Lead contact

Further information and requests for data should be directed and will be fulfilled by the lead contact, Dimitrios Vavylonis (vavylonis@ lehigh.edu).

Materials availability

This study did not generate new unique reagents.

Data and code availability

- The initialization files to reproduce the simulations reported in this paper have been deposited at Zenodo and are publicly available as of the date of publication. DOIs are listed in the key resources table. Molecular dynamics trajectory files will be available without restrictions from the lead contact.
- This paper does not report original code.
- Any additional information required to reanalyze the data reported in this paper is available from the lead contact upon request

METHOD DETAILS

Systems

We make use of the crystal structure of Mid1, PDB: 4XOH9 using the 'A' structure and filling in all residues missing in sequence 580-920 using I-TASSER³⁶ (C2-PH). For simulations of only a section of C2-PH, we simply removed the unneeded residues lines from the filled-in PDB file. Lipid models selected for POPIP2 included half protonated on the P4 and half on the P5 (CHARMM-GUI models POPI24 & POPI25). Other membrane component models were chosen as named in Figure 1C. Systems were initialized with box sizes and atom counts as described in Table 1 (Figure S3). For the C2-PH unbound systems the protein was started in a different rotational orientation for each independent simulation sampled from an approximately uniformly spherical distribution. For other systems, the replicas begin from the same initial condition but diverge due to differing random number seeds. The number of repeats is shown in Table 1.

C2-PH dimer systems were initialized using structures obtained near the end of monomer trajectories. For a given monomer/membrane structure, the solvent and ions were removed. A structure of the Mid1 dimer from (Figure S2A) was aligned to the monomer in VMD⁵² using the C2 interfacial residues as shown in Figure S2B. The monomer containing the residues used for alignment was removed from the system, leaving the original monomer in the trajectory and a partner monomer bound via the interfacial residues. Solvent and ions were added back to the system using the GROMACS commands solvate and genion.





MD simulations

All systems were prepared using CHARMM-GUI⁵³ Membrane Builder^{54–57} exporting inputs for GROMACS.^{58,59} Simulations were performed using the CHARMM36(m) force field^{58,60} in GROMACS versions 2018.5 and 2020.4⁶¹ using the TIP3P water model⁶² with 100 mM KCI. Equilibration and production simulations were performed largely as prescribed by the GROMACS inputs generated by CHARMM-GUI. Relaxation included an energy minimization step of 5000 steps using the steepest descent algorithm. Following this, the system was simulated in the NVT (constant particle number, volume, and temperature) ensemble for 250 ps with a 1 fs time step. Then the system was switched to an NPT (constant particle number, pressure, and temperature) ensemble with 1 fs time step for 125 ps, and then a 2 fs time step for 1.5 ns. During equilibration, positional and dihedral restraints were used with gradually decreasing force constants. The duration of equilibration steps was increased for individual cases if needed. Production simulations were performed unrestrained in the NPT ensemble with a 4 fs time step using hydrogen mass repartitioning. 63 Some dimer and CH simulations used a 3 fs time step to improve stability as needed. Temperature was maintained at 300 K with a Nosé-Hoover thermostat with a time constant of 1 ps. Pressure was maintained at 1 bar with a semi-isotropic Parrinello-Rahman barostat with compressibility of 4.5×10^{-5} bar⁻¹ and time constant of 5 ps for the unbound C2-PH case, which was increased for all other simulations to 12 ps to improve stability. Systems were visualized in VMD.⁵²

QUANTIFICATION AND STATISTICAL ANALYSIS

Contact analysis was done in python using the *compute_neighbors* function of the MDTraj package. ⁶⁴ Contacts were defined with a 5 Å cutoff. Helix propensity was calculated using DSSP^{65,66} using the GROMACS command do_dssp and grouping helixes of the G, H, and I designations (3, 4, and 5 turn helixes respectively). Orientation analysis was done in python using the first principal component as calculated by the principal command in GROMACS.